

# Gamma Irradiation Effects on Physical, Optical, Structural and Radiation Shielding Properties of Tellurite-Based Glasses

Huan Koh, Floressy Juhim, Fuei Pien Chee\*

\*fpchee06@ums.edu.my

Faculty of Science and Natural Resources, University Malaysia Sabah, 88400 Sabah, Malaysia

Received: June 2024

Revised: February 2025

Accepted: March 2025

DOI: 10.22068/ijmse.3636

**Abstract:** Tellurite glasses have been researched for their radiation shielding properties as a potential alternative to lead and lead silica glass, which poses toxicity concerns. The effects of radiation on tellurite glasses are assessed using physical irradiation and simulation with the Phy-X/PSD software. Glasses with the composition  $(70-x-y) \text{TeO}_2-20\text{ZnO}-9\text{Na}_2\text{O}-1\text{Er}_2\text{O}_3-(x)\text{TiO}_2-(y)\text{Al}_2\text{O}_3$ , were fabricated using the melt-quench method. These glasses were then irradiated with gamma radiation at different doses. Characterization techniques, including X-ray diffraction (XRD), UV-VIS spectroscopy, and density measurements, were applied to the glasses before and after irradiation. The XRD results confirmed that the glass samples were amorphous. UV-VIS spectroscopy showed that transmittance decreased as the radiation dose increased. The Phy-X/PSD simulation program was used to model the radiation properties of the glasses based on their dosage and composition. The simulation results indicated that the half-value layer (HVL) and mean free path (MFP) increased post-irradiation and remained constant. These findings suggest that tellurite glasses, which have enhanced radiation-shielding properties, could be a viable, safer alternative to lead-based glasses for various applications.

**Keywords:** Tellurite glass, Titanium NPs, Aluminium oxide NPs, Gamma, Phy-X/PSD simulation.

## 1. INTRODUCTION

Ever since the advent of nuclear technology, the need for radiation-resistant glasses has grown steadily, driven by the expanding development and presence of radiation sources. The increase in space exploration has further necessitated the production of these specialized glasses [1]. In space, the absence of an atmospheric layer to protect astronauts and their equipment from radiation makes the problem even more pronounced, as all forms of radiation can easily penetrate materials without such protection.

Additionally, medical technology has seen significant growth in the use of radiation for both treatment and diagnostic purposes, underscoring the need for advanced radiation-resistant materials. These applications demand materials that effectively shield against harmful radiation while maintaining their structural integrity and optical properties. Developing radiation-resistant glasses is crucial for ensuring safety and performance in a wide range of environments, from space missions to medical facilities [2].

As a result of the wide use of radiation technology, numerous methods of resisting radiation for a human user in these circumstances have been developed. In the medical field, lead aprons are often used to shield the patient and medical

personnel alike when conducting radiation-based scanning of the body, such as x-ray and MRI; and when receiving radioactive medicine, such as radiotherapy. In nuclear reactors, thick concrete walls are constructed around the reactor, and the administration and control buildings have extra thick walls. Spacecraft also use metal casings to shield the components and the astronauts from unfiltered radiation from space. All these methods leave little to no room for visibility through the shielding [3]. Thus, the material's radiation sensitivity must be thoroughly researched before it is subjected to a radiation environment [4].

Hence, a glass with radiation-resistant properties that is transparent enough to look through and easy to manufacture has been highly requested [5]. Silicate-based glasses lined with lead oxides have been used for radiation protection. Lead glasses are commonly used; however, the lead content has reduced the melting point and hardness of the glass. In addition to the environmental issues resulting from using lead, alternatives must be developed [6]. On that account, a prominent element for this research has been Tellurite. Tellurite exhibits desirable chemical and physical properties such as low melting point, low phonon energy, low crystallization ability, high dielectric constant, and high thermal stability [7]. There have been several investigations into tellurite

glass compositions, such as erbium-doped tellurite glass [8, 9], tellurite glass with zinc fluoride nanoparticles [10], and titania-bismuth-borotellurite glass [11]. In particular, there is interest in developing compositions containing titania and aluminium oxide nanoparticles [12–15]. Furthermore, radiation damage to the tellurite glass system has received significant attention in recent studies for radiation shielding applications [16].

In the study, glass samples were discovered to be transparent based on optical properties [17]. It is light yellow with a concentration of 10 mol%  $\text{TeO}_2$ . It began to obtain a much darker colour with rising  $\text{TeO}_2$  concentration before it became dark red [17]. In another study of the tellurite glass system at ambient temperature, a  $^{60}\text{Co}$  gamma cell (2000 Ci) was employed as a gamma-ray source with a dosage rate of  $1.5 \text{ Gy s}^{-1}$  ( $150 \text{ rad s}^{-1}$ ). After irradiation, the colour of a glass system changed from transparent yellow to brown [18]. The acquired spectra reveal that all edges display a redshift as the radiation dose increases. The resistance level to gamma-irradiation depends on the redox potential of the individual ions [18].

Furthermore, alternative methods to test the effects of radiation are being researched, which have the potential to replace direct testing using actual radiation. These methods include simulation by computer programs such as Phy-X/PSD, among others. For this research, the simulation program Phy-X/PSD is used. Phy-X/PSD is a web-based simulation program easily accessible at the address <https://phy-x.net/PSD>. It was developed by Sakar et al. in 2020. The program is capable of simulating a range of radiation energies, as well as some well-known radioisotopes' energies. The number of types of material being simulated is also virtually infinite as the input can be any combination of the periodic table and its corresponding density.

Phy-X/PSD is relatively new to the scene of radiation and particle simulation programs. Thus, the study of its suitability and usage in research is ongoing. It has been determined that Phy-X/PSD can be used as one of the theoretical approaches to calculate the photon attenuation factors [3]. Other than that, it is noted that the program is fast and accurate in its calculations. The database computes the parameters through the chemical formula and the density of the

glass specimens [5]. The output of these calculations can then be saved as an Excel file by the user.

In this work, the tellurite glass with a composition of  $(70-x-y) \text{ TeO}_2-20\text{ZnO}-9\text{Na}_2\text{O}-1\text{Er}_2\text{O}_3-(x)\text{TiO}_2-(y)\text{Al}_2\text{O}_3$ , with a total mass of 20 g per glass sample, was fabricated. Analysis was then performed on the physical, structural, and optical properties pre- and post-irradiation, along with simulating the radiation analysis using Phy-X/PSD. The irradiation is done separately for each sample with total ionizing doses (TID) of 5, 10, 50, 75, and 100 kGy.

## 2. EXPERIMENTAL PROCEDURES

### 2.1. Fabrication of Glass

In this project, two samples were prepared using a conventional melt quenching process. The raw materials obtained from Sigma Aldrich, included tellurium dioxide ( $\text{TeO}_2$ , purity 99%), zinc oxide ( $\text{ZnO}$ , purity  $\geq 99\%$ ), sodium oxide ( $\text{Na}_2\text{O}$ , purity 80%), erbium III oxides ( $\text{Er}_2\text{O}_3$ , purity  $>99.99\%$ ), titanium IV oxide ( $\text{TiO}_2$ , with a primary particle size of 21 nm, purity  $\geq 99.5\%$ ), and aluminium oxide nanopowder ( $\text{Al}_2\text{O}_3$ , with a primary particle size of 13 nm, purity 99.8%) with a total mass of 20 g per glass sample. The samples were prepared with the compositions of  $(70-x-y) \text{ TeO}_2.20\text{ZnO}.9\text{Na}_2\text{O}.1\text{Er}_2\text{O}_3.(x)\text{TiO}_2.(y)\text{Al}_2\text{O}_3$ , where the sample with code TZNETA3 having  $x = 0.3 \text{ mol}\%$  and  $y = 0.6 \text{ mol}\%$  and the sample with code TZNETA6 having  $x = 0.6 \text{ mol}\%$  and  $y = 0.3 \text{ mol}\%$ . The composition masses are listed in Table 1. A platinum crucible containing the materials was prepared and melted in an electrical furnace at  $950^\circ\text{C}$  for 30 min. The mixture was then poured into a brass mould and held at  $250^\circ\text{C}$  for annealing for 3 h.

The samples were then characterized before and after irradiation. The samples were sent to the Malaysia Nuclear Agency, with the specific facility of MINTec-SINAGAMA Irradiation Plant. This facility uses ionizing energy in the form of gamma radiation with Cobalt-60 as its source. The samples were brought to the plant for irradiation, specifically utilizing the JS10000 IR 219 tote irradiator system with an irradiation rate of  $2 \text{ kGy/h}$ . Then, the samples were irradiated with TID of 5, 10, 50, 75, and 100 kGy, each dose applied separately to individual samples, using an average gamma energy of 1.25 MeV.

**Table 1.** Chemical composition of glass samples

Glass code	TZNETA3		TZNETA6	
	(mol%)	Mass (g)	(mol%)	Mass (g)
TeO <sub>2</sub>	69.1	16.122	69.1	16.129
ZnO	20	2.379	20	2.380
Na <sub>2</sub> O	9	0.815	9	0.816
Er <sub>2</sub> O <sub>3</sub>	1	0.559	1	0.559
TiO <sub>2</sub>	0.3	0.035	0.6	0.070
Al <sub>2</sub> O <sub>3</sub>	0.6	0.089	0.3	0.045
Total	100	20	100	20

The ceric-cerous dosimeter was used to analyze the radiation dose absorbed by all samples, and the Total Ionizing Dose (TID) in these studies was verified based on the evaluation of the ceric-cerous system for gamma radiation exposure. When exposed to ionising radiation, this dosimetry system operates based on the oxidation-reduction reaction between ceric (Ce<sup>4+</sup>) ions and cerous (Ce<sup>3+</sup>) ions in an acidic solution. The radiation-induced reduction of Ce<sup>4+</sup> to Ce<sup>3+</sup> results in a measurable change in optical absorbance, typically monitored using spectrophotometry. The glass samples were exposed to Co-60 gamma radiation (1.25 MeV) at various TID, and structural and optical changes were analyzed before and after irradiation.

The density of the glass samples, with 2 samples each for pre- and post-irradiation, was measured. The density of the glass was determined using an analytical balance of specific density-PrecisaXT220A. The density of the glasses was calculated using the suspended weight method based on Archimedes' principle at room temperature and computed using equation (1). The calculation for the density of the samples is then expressed as:

$$\rho = \frac{W}{|W_d|}(\rho_0 - d) + d \quad (1)$$

Where  $\rho$  is the density of the sample,  $W$  is the weight of the sample in air,  $W_d$  is the difference between the weight of the sample in air and water,  $\rho_0$  is the density of water at 29°C (0.99651 g/cm<sup>3</sup>), and  $d$  is a constant.

Model Lambda UV-VIS spectroscopy EZ210 was used to achieve UV-VIS spectroscopy of the proposed glasses. The glass samples' optical transmittance was measured before and after irradiation. The optical energy gap and radiation-induced absorption can be calculated using these transmittance measurements in the UV and visible spectral ranges [19].

Bruker D2 Phaser was used to achieve XRD

analysis of the proposed glasses. After this, the data is extracted to acquire the intensity peak graph. Corresponding peaks in the graph were then identified for their respective structures [20].

## 2.2. Radiation Shielding Properties

PSD, which stands for Photon Shielding and Dosimetry, is a simulation software made available online at <https://phy-x.net/PSD>. This software was developed to calculate parameters related to shielding and dosimetry. Some of these parameters include the mass attenuation coefficient (MAC), half value layer (HVL), adequate atomic number ( $Z_{\text{eff}}$ ), and energy absorption buildup factor (EABF). The software can generate data on the shielding parameters in the continuous energy region of 1 keV to 100 GeV and some well-known radioactive sources such as Cobalt-60, Caesium-137, Sodium-22, and Iodine-131. The user can select the energy ranges to be tested at will, depending on their research requirements. The material being tested can also be inserted by the user by inputting the composition and the density of the material.

Phy-X/PSD runs on a remote server with Intel® Core™ i7-2600 CPU @ 3.40 GHz CPU with 1 GB installed memory and its operating system being Ubuntu 14.03.3 LTS. The application language is NodeJS v8.4.0, serving with Nginx 1.15.8. Security between the client's browser and the server is being established with 256 Bit Positive SSL [21].

Direct measurement of gamma-ray absorption in glass requires specialized instruments such as gamma spectroscopy, which may not always be available. Instead, this study used the Phy-X/PSD software, a well-validated technique for computing shielding parameters based on the glass's elemental composition and density. The software calculates important shielding parameters such as Mass Attenuation Coefficient (MAC), which measures the likelihood of gamma photon interactions

with the material. Half-Value Layer (HVL) is the thickness necessary to reduce gamma intensity in half, while Mean Free Path (MFP) is the average distance gamma rays travel before interacting with the material. These measurements provide an indirect but reliable assessment of the glass's efficiency as a gamma shield.

### 2.2.1. Mass attenuation coefficient (MAC)

The mass attenuation coefficient is the probability per unit mass that a photon will interact with the material through absorption or scattering. Thus, this number is often presented as a fraction. The MAC can be derived from the Beer-Lambert law, which is the relationship between the attenuation of light through a substance and the properties of that substance [22]. The relationship can be expressed in the form of Equation (2) [23]:

$$I = I_0 e^{-\mu x} \quad (2)$$

Where  $I$  is the incident intensity,  $I_0$  is the transmitted intensity,  $\mu$  is the linear mass coefficient, and  $x$  is the thickness.

We can then use this to calculate the mass attenuation coefficient by using the relation of Equation (3) [23]:

$$\mu_m = \frac{\mu}{\rho} \quad (3)$$

Where,  $\mu_m$  is the mass attenuation coefficient and  $\rho$  is the density

When used with MFP and HVL, the relations then become Equations (4) and (5) [23]:

$$\text{MFP} = \frac{1}{\mu} \quad (4)$$

$$\text{HVL} = \frac{\ln 2}{\mu} \quad (5)$$

### 2.2.2. Mean free path (MFP)

The mean free path is defined as the average distance a photon travels before an interaction

occurs, such as a change in direction or a change in velocity. From this relation, we can say that the lower the MFP value, the better the resistance against radiation. The photon loses energy as it interacts with the medium, reducing its penetrating power as well.

### 2.2.3. Half-value layer (HVL)

The half value layer is defined as the thickness of the material where half the intensity of the incident photon is maintained [23]. In simpler terms, HVL is the length of the material at which the penetrating photon reduces its intensity by half [23]. This indicates that the lower the HVL value, the better the resistance against radiation. As the photon's energy is halved by an increasingly thinner material, the penetrating power of the photon when it exits the material reduces significantly as well. This means we can fabricate a thinner glass, thus saving on material and cost while providing sufficient radiation shielding.

## 3. RESULTS AND DISCUSSION

### 3.1. Structural Properties

#### 3.1.1. XRD

The samples were crushed finely using an agate mortar and pestle and packed in a conical tube. The amorphousness of the glass is analysed using XRD. Fig 1 shows the XRD spectra of glass with varying dosages of gamma radiation between samples TZNETA3 and TZNETA6, respectively. The appearance of broad diffuse scattering located at 25–35 degrees without sharp crystallization peaks signifies the amorphous nature and indicates the short-range order of atoms in the glass [12].

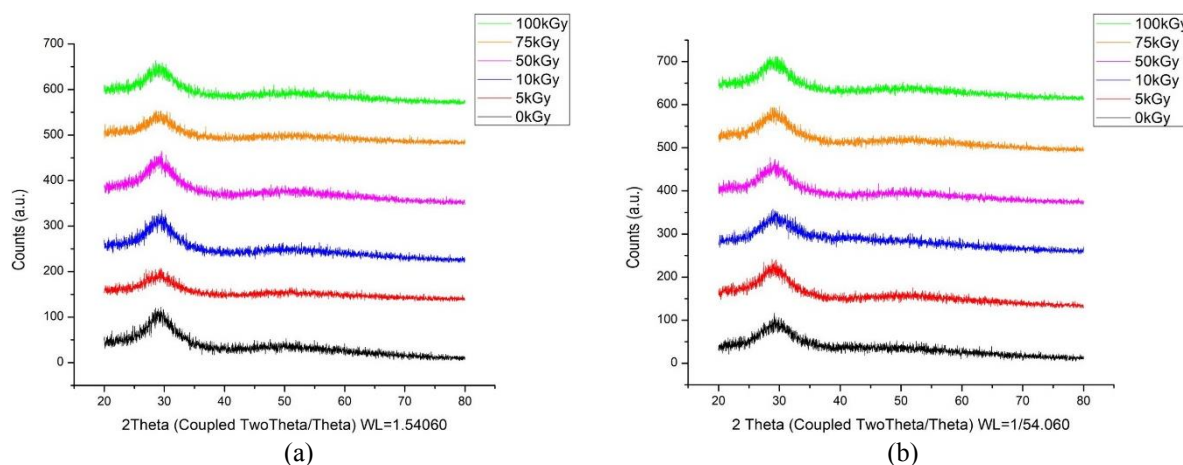


Fig. 1. XRD spectra of a) TZNETA3 and b) TZNETA6



The XRD patterns recorded are identical based on Fig 1 before and after gamma rays. As a result, the XRD patterns confirm the existence of an amorphous glass system [24].

### 3.1.2. Density

The density for TZNETA3 decreases immediately once irradiated. The data has slight changes between  $5.13396 \text{ gcm}^{-3}$  to  $5.14515 \text{ gcm}^{-3}$  post-irradiation, as shown in Fig 2 and detailed in Table 2. This indicates that the damage done to the glass is immediate and constant regardless of the amount of dosage applied. This is due to the energy being constant through all dosages, which is at 1.25 MeV. When bonds between oxygen and network-forming atoms break, the oxygen atoms may not make new links immediately. These unbound oxygen atoms, known as non-bridging oxygens (NBOs), remain within the glass structure. NBOs can affect the physical qualities of glass, such as density. Density changes occur as atoms rearrange and voids emerge, altering the material's compactness.

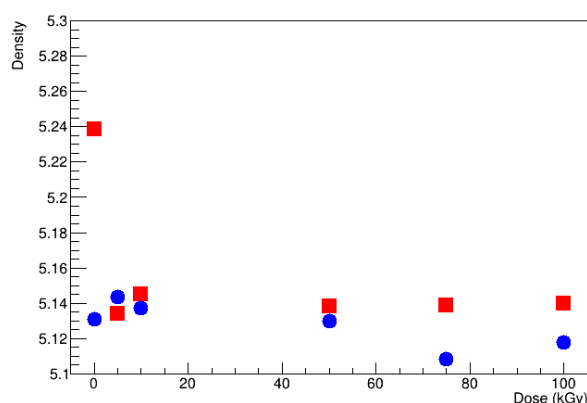


Fig. 2. Density of TZNETA3 and TZNETA6 pre- and post-irradiation

Table 2. Density of samples

Dosage (kGy)	TZNETA3	TZNETA6
Not Irradiated (0)	5.21758	5.13083
5	5.13396	5.14365
10	5.14515	5.13737
50	5.13814	5.12997
75	5.13875	5.10825
100	5.14008	5.11774

The dosage does not affect the penetrative power of the radiation, which is only affected by the irradiation energy. A study found that the penetrating power is correlated with the irradiation energy, with a weak energy stopping

within the sample and an intense energy penetrating the sample entirely [25]. Since the energy is constant throughout the irradiation process at 1.25 MeV, the penetration of the radiation on the glass samples is steady, and the damage done is on the same layers on all samples. Thus, the density remains constant post-irradiation.

The initial trend for the TZNETA6 sample increases instead of decreases, while the post-irradiation readings vary slightly between  $5.10825 \text{ gcm}^{-3}$  and  $5.14365 \text{ gcm}^{-3}$ . This is due to the outliers in the density of the glass pre-irradiation, where the average is taken for comparison pre- and post-irradiation analysis. These minor differences are important indicators that the structural damage is mostly caused by void creation and atomic reconfigurations.

As the dose continues to increase, there is a very slight decrease in the density of the glass. This is attributed to the expansion that occurs in the glass, which comes from the formation of voids [26]. According to Ruller and Friebele (1991) [27], voids are produced when electrons or holes formed by ionization in the network are trapped. As a result, it will cause the bond to rupture or increase in length. The formation of voids is a complex process that must take into account many factors, such as the chemical composition and the microstructure of the material. The samples investigated here created voids by the ionization of the atoms, which breaks the bonds between the atoms and causes them to be pushed around into the interstitial space. When enough atoms experience this effect, the space left behind creates a void.

### 3.2. Optical Properties

The optical properties in the spectra range of 400-1000 nm were analysed by the ultraviolet-visible (UV-VIS) spectroscopy using Model Lambda EZ210. Fig 3 and 4 show the UV-VIS absorption and transmission spectra of the glass samples of TZNETA6 and TZNETA3. Generally, the spectral features of both sample series were found to be qualitatively similar. The absorption peaks were attributed to structural rearrangements of the glass due to the 4f-4f transition in the erbium ions in the glass matrix [28].

Seven absorption peaks were observed, centered at different wavelengths, and their corresponding erbium transitions are summarized in Table 3.

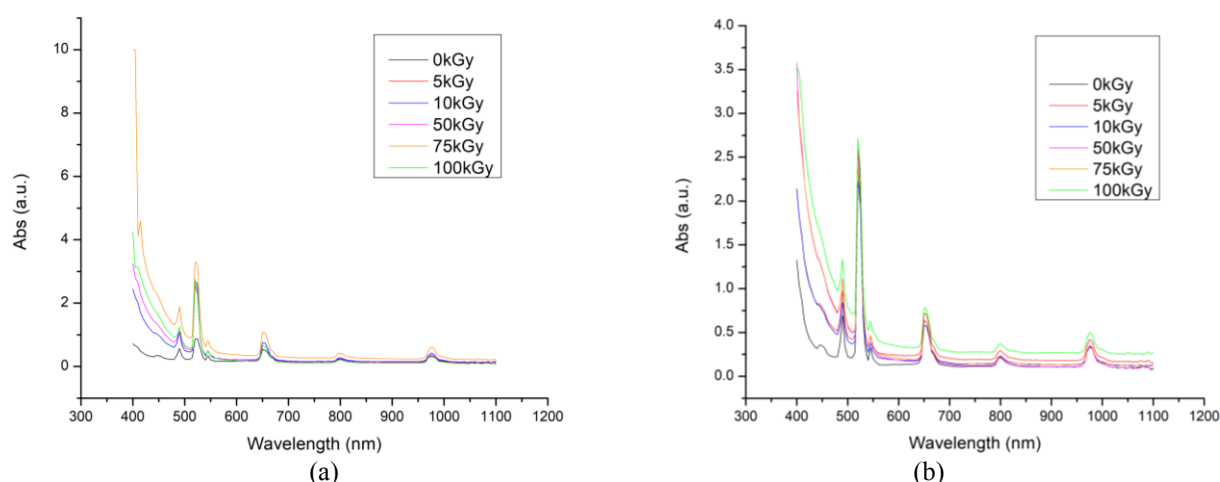


**Fig. 3.** UV-VIS absorption spectra for a) TZNETA3 and b) TZNETA6

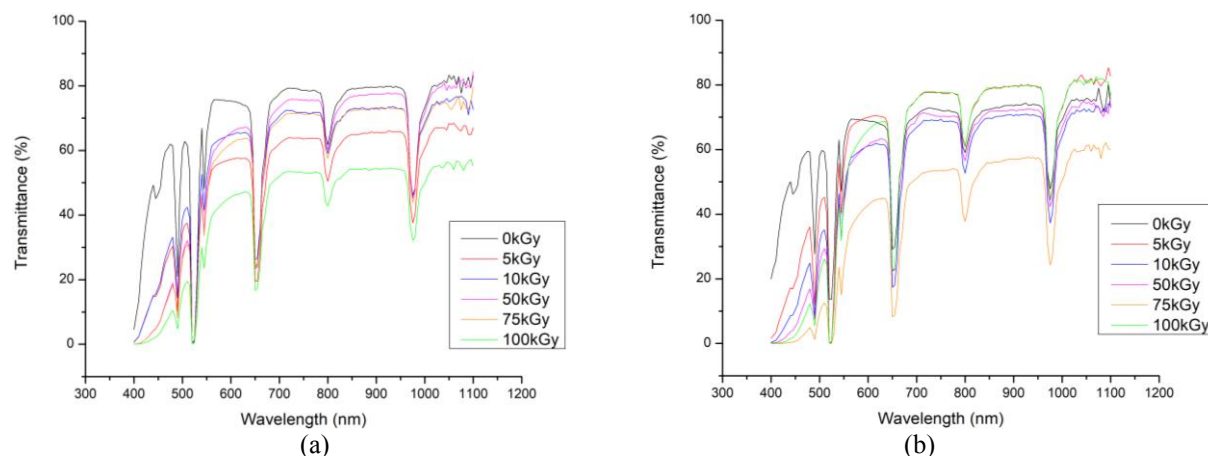


**Fig. 4.** UV-VIS transmittance spectra of a) TZNETA3 and b) TZNETA6

The transition of the erbium ions was tabulated based on energy value referring to energy levels of trivalent lanthanide aquo ions [29].

**Table 3.** Absorption peaks centre and corresponding Erbium transitions

Absorption band centre (nm)	Erbium transition energy level
445	$^4F_{3/2}$
490	$^4F_{7/2}$
519	$^2H_{11/2}$
545	$^4S_{3/2}$
650	$^4F_{9/2}$
800	$^4I_{9/2}$
975	$^4I_{11/2}$

The absorption spectra consist of seven absorption bands centred around the wavelengths of 445, 490, 519, 545, 650, 800, and 975 nm. These peaks represent the transition of erbium

ions from ground state  $^4I_{15/2}$  to excited state energy levels of  $^4F_{3/2}$ ,  $^4F_{7/2}$ ,  $^2H_{11/2}$ ,  $^4S_{3/2}$ ,  $^4F_{9/2}$ ,  $^4I_{9/2}$ , and  $^4I_{11/2}$  respectively [8].

A study found additional absorption bands at 554 nm and 827 nm, corresponding to the Ti and Al atoms, respectively. However, these weak bands reflect the inconsistent symmetry in the distribution of the nanoparticles (NPs). The absence of these bands in the present data is also due to the small resolution of the acquired data, which means that the bands are insignificant when compared to the intensity of the peaks made by the erbium ions [12]. The bands acquired in this study were obtained by fabricating a separate series of samples that excluded  $Er_2O_3$  from the composition. Thus, the bands are clearer than those with erbium ions.

In the transmittance spectra for the TZNETA6 sample, there is a decrease in the transmittance as the dosage increases, with the exception of 75

kGy being the lowest. Meanwhile, the transmission spectra for the TZNETA3 sample also decrease except for the 5 kGy sample. As the energy increases, the transmittance of the glass decreases due to the damage done. According to the research by [30], the effects of gamma radiation on optical properties of glass with a composition of  $\text{CeO}-\text{Na}_2\text{O}-\text{SrO}-\text{B}_2\text{O}_3$  is investigated. The data acquired here corresponds to the findings of [30] in that the transmission of the glass samples was decreased after exposure to gamma irradiation in all wavelengths.

The damage done to the glass is caused by the ionization of the atoms in the glass, which comes from 3 types of interactions of gamma rays with the atoms: the photoelectric effect, the Compton effect, and pair production. These contribute to the calculation of the total absorption coefficient [31]. Additionally, the ionization of the atoms also causes the formation of non-bridging oxygens (NBO). This process causes the chemical bonds to break, releasing oxygen atoms and ions, which then enter the interstitial spaces in the glass network, becoming interstitial atoms. The atoms then become bonded to the nearest atoms, which is the tellurite network, causing the  $\text{TeO}_3$  units to change into  $\text{TeO}_4$  trigonal bipyramids, which contribute to the alteration of the other properties of the glass [32].

The alterations to the glass structure and network cause the optical properties to change as well. The formation of NBO's increases the interaction of the light rays entering the glass sample. This then causes the absorption spectra to increase as the higher the dosage, the more the NBO's are formed due to the increasing damage. The increase in absorption can also be due to the generation of additional erbium ions from irradiation. When a glass containing a transition or rare earth ions is irradiated, the ions act as a trap for released electrons and holes during the irradiation process [33]. Thus, in general, we can say that the higher the energy, the higher the interaction with atoms, and the higher the absorption.

Other defects are also found to be an effect of the irradiation. The generation of O-centres after gamma irradiation causes too many additional absorption effects. These effects come in the form of additional absorption spectra and peaks at certain wavelengths [33]. It is then concluded that the overlap of multiple damages and defects contributes to the increase of amplitude and

bandwidth in absorption, thereby decreasing the transmittance of the glass sample.

The damage from the irradiation is also found to be permanent and irreversible. This is due to the non-conducting nature of the material, where mobility of the defects is very small or negligible.

### 3.3. Radiation Properties

The trend for HVL and MFP of the samples pre- and post-irradiation can be seen in Fig 5. In general, the values for HVL and MFP increase as the sample is irradiated and then are constant through all the dosages. This is due to the decrease in density as irradiation increases. It is noted that the HVL and MFP are inversely proportional to the density of the sample. In particular, the sample TZNETA3 increases its HVL value from 2.4775 to 2.5175 cm at 5 kGy dose irradiation, while the sample TZNETA6 initially decreases its HVL value from 2.5195 to 2.5130 cm at 5 kGy dose irradiation but then increases again to its highest point of 2.5305 cm at 75 kGy dose irradiation. The MFP shows a similar trend in that the value for the TZNETA3 sample increases from 3.5740 to 3.6315 cm at 5 kGy dose irradiation, while the TZNETA6 sample initially decreases from 3.6350 to 3.6260 cm at 5 kGy dose irradiation but then increases again to its highest point of 3.6510 cm at 75 kGy dose irradiation.

The values also remain relatively constant for all readings post-irradiation, with the range between values being 0.0025 cm and 0.0175 cm in HVL, along with 0.0070 cm and 0.0250 cm in MFP for TZNETA3 and TZNETA6, respectively. This trend is not affected by the dosage but instead is due to the constant penetrative power as energy was constant during irradiation.

The MAC of all samples are observed to be the same. The MAC is determined by the theoretical composition of the sample only. Thus, any changes induced by the irradiation are irrelevant in this case. Table 4 lists the mass attenuation coefficients (MAC), half value layer (HVL), and mean free path (MFP) of the glass samples against the increasing radiation dosage by result of the Phy-X/PSD simulation.

In comparison, the density of the glasses influences properties such as HVL, TVL, and MFP, whereas the MAC value has direct connections with experimental results across a range of TID.

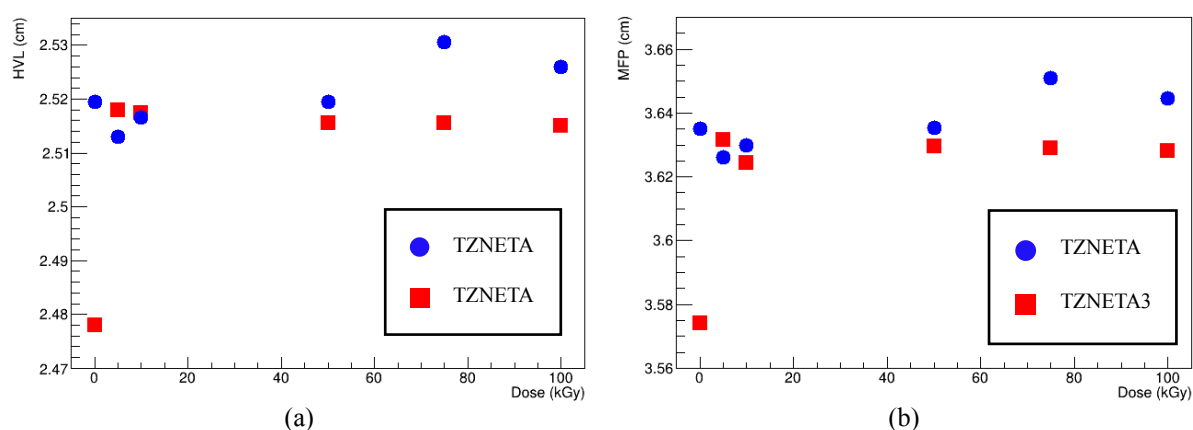


**Fig. 5.** Graph of a) HVL and b) MFP TZNETA3 and TZNETA6 pre- and post-irradiation

**Table 4.** MAC, HVL, and MFP readings from Phy-X/PSD of TZNETA3 and TZNETA6 pre- and post-irradiation

Dosage (kGy)	MAC		HVL (cm)		MFP (cm)	
	TZNETA3	TZNETA6	TZNETA3	TZNETA6	TZNETA3	TZNETA6
Not Irradiated (0)	0.054	0.054	2.4775	2.5195	3.5740	3.6350
5	0.054	0.054	2.5175	2.5130	3.6315	3.6260
10	0.054	0.054	2.5175	2.5165	3.6245	3.6300
50	0.054	0.054	2.5155	2.5195	3.6295	3.6355
75	0.054	0.054	2.5155	2.5305	3.6290	3.6510
100	0.054	0.054	2.5150	2.5260	3.6280	3.6445

While direct gamma absorption measurements are ideal, a material's shielding performance is mostly determined by its composition and density, which were thoroughly tested in this study. The agreement between theoretical (Phy-X/PSD) and experimental (irradiation-induced alterations) results confirms the glass's radiation shielding capability. The investigated glasses have a higher MAC than tellurite glasses containing  $\text{Sm}_2\text{O}_3$  and  $\text{Nd}_2\text{O}_3$  [34] and chalcogenide glasses [35]. The photon shielding characteristics of the glasses improve with increased NP content. This study demonstrates that the examined glasses can be used as radiation shielding materials even under high TID gamma irradiation.

#### 4. CONCLUSIONS

This study examined the physical, optical analysis, and radiation characteristics of glass through both physical experimentation and software simulation, exploring the correlation between these methods. Observations showed that the physical properties of the glass remained relatively stable across all samples immediately post-irradiation. However, post-irradiation optical analysis revealed a decreasing trend with increasing radiation dosage, attributed to cumulative radiation

damage. In contrast, the radiation analysis indicated that the trend increased immediately post-irradiation and then stabilized, highlighting a discrepancy between the optical and radiation responses due to the differing nature of damage accumulation and energy variation. The glass's shielding efficiency is effectively evaluated using validated computational methods (Phy-X/PSD) and experimental irradiation studies. The results show that the glass composition and density provide adequate gamma-ray attenuation. The findings suggest that continued investigation of tellurite glass containing NPs is a viable alternative for radiation shielding materials. Additionally, the absence of toxic materials in tellurite glass enhances its appeal. Utilizing simulation programs for material testing against radiation proves advantageous, as it minimizes radiation exposure and allows comprehensive monitoring of variables and results. Nevertheless, further testing is essential to validate the accuracy of the simulation program's results.

#### ACKNOWLEDGEMENT

The authors would like to extend their gratitude to the Malaysia Ministry of Higher Education for their support in funding this research under the



Fundamental Research Grant Scheme (FRGS) Year 2022 with the grant code, FRGS/1/2022/STG07/UMS/02/1.

## REFERENCES

- [1]. Zhang, F., Cao, X., Ma, Y., Zhang, Z., Huo, W., Wan, R., Yang, L., Gao, F., & Wang, P., "Enhancement of the radiation resistance of cerium-containing fluorophosphate glasses through codoping with  $\text{Sb}_2\text{O}_3$  and  $\text{Bi}_2\text{O}_3$ ". *Ceramics International*, 2022, 48(14), 20041–20052. <https://doi.org/10.1016/j.ceramint.2022.03.280>.
- [2]. AlMisned, G., Sen Baykal, D., Alkarrani, H., Susoy, G., & Tekin, H. O., "Advancing mechanical durability and radiation shielding properties in Silicon dioxide ( $\text{SiO}_2$ ) glasses through various incorporations: A comparative analysis". *Results Phys*, 2024, 61(March), 107717. <https://doi.org/10.1016/j.rinp.2024.107717>.
- [3]. Al-Hadeethi, Y., & Sayyed, M. I., "A comprehensive study on the effect of  $\text{TeO}_2$  on the radiation shielding properties of  $\text{TeO}_2\text{-B}_2\text{O}_3\text{-Bi}_2\text{O}_3\text{-LiF-SrCl}_2$  glass system using Phy-X/PSD software". *Ceramics International*, 2020, 46(5), 6136–6140. <https://doi.org/10.1016/j.ceramint.2019.11.078>.
- [4]. Rasmidi, R., Mivolid, D. S., Chee, F. P., Juhim, F., Rumaling, M. I., Salleh, S., Eswar, K. A., Salleh, K. A. M., Ibrahim, S., "Structural and Optical Properties of TIPS Pentacene Thin Film Exposed to Gamma Radiation". *Materials Research*, 2022, 25, 1–7. <https://doi.org/10.1590/1980-5373-MR-2022-0227>.
- [5]. A Aşkın, A., Sayyed, M. I., Sharma, A., Dal, M., El-Mallawany, R., & Kaçal, M. R., "Investigation of the gamma ray shielding parameters of  $(100-x)[0.5\text{Li}_2\text{O}-0.1\text{B}_2\text{O}_3-0.4\text{P}_2\text{O}_5]\text{-xTeO}_2$  glasses using Geant4 and FLUKA codes". *Journal of Non-Crystalline Solids*, 2019, 521(May), 119489. <https://doi.org/10.1016/j.jnoncrysol.2019.119489>.
- [6]. "Using Glass for Radiation Shielding", Krista Grayson, December 2020, <https://mo-sci.com/using-glass-for-radiation-shielding>.
- [7]. Sayyed, M. I., "Bismuth modified shielding properties of zinc boro-tellurite glasses. *Journal of Alloys and Compounds*". *Journal of Alloys and Compounds*, 2016, 688, 111–117. <https://doi.org/10.1016/j.jallcom.2016.07.153>.
- [8]. Awang, A., Ghoshal, S. K., Sahar, M. R., Arifin, R., & Nawaz, F., "Non-spherical gold nanoparticles mediated surface plasmon resonance in  $\text{Er}^{3+}$  doped zinc-sodium tellurite glasses: Role of heat treatment". *Journal of Luminescence*, 2014, 149, 138–143. <https://doi.org/10.1016/j.jlumin.2014.01.027>.
- [9]. Yusof, N. N., Ghoshal, S. K., & Azlan, M. N., "Optical properties of titania nanoparticles embedded  $\text{Er}^{3+}$ -doped tellurite glass: Judd-Ofelt analysis". *Journal of Alloys and Compounds*, 2017, 724, 1083–1092. <https://doi.org/10.1016/j.jallcom.2017.07.102>.
- [10]. Ahmmad, S. Kareem, Samee, M. A., Edukondalu, A., & Rahman, S., "Physical and optical properties of zinc arsenic tellurite glasses". *Results in Physics*, 2012, 2, 175–181. <https://doi.org/10.1016/j.rinp.2012.10.002>.
- [11]. Donya, H., & Sulami, S., "Photon Shielding Characterization of a Modified Titania-Bismuth-Borotellurite Glass System for Medical Applications". *Journal of the Korean Physical Society*, 2019, 75(11), 871–877. <https://doi.org/10.3938/jkps.75.871>.
- [12]. Ferodolin, I., Awang, A., Ghoshal, S. K., Samavati, A., Pien, C. F., & Dayou, J., "Plasmonic effect of bimetallic  $\text{TiO}_2/\text{Al}_2\text{O}_3$  nanoparticles in tellurite glass for surface-enhanced Raman scattering applications". *Journal of Luminescence*, 2022, 241 (February 2021), 118488. <https://doi.org/10.1016/j.jlumin.2021.118488>.
- [13]. Juhim, F., Chee, F. P., Awang, A., Moh, P. Y., Mohd Salleh, K. A., Ibrahim, S., Dayou, J., Alalawi, A., Al-Buriahi, M. S., "Study of gamma radiation shielding on tellurite glass containing  $\text{TiO}_2$  and  $\text{Al}_2\text{O}_3$  nanoparticles". *Heliyon*, 2023, e22529. <https://doi.org/10.1016/j.heliyon.2023.e22529>.
- [14]. Ali, A. M., Issa, S. A. M., Ahmed, M. R., Saddeek, Y. B., Zaid, M. H. M., Sayed, M., Somaily, H. H., Tekin, H. O., Sidek, H. A. A., Matori, K. A., Zakaly, H. M. H.,

- "Promising applicable heterometallic  $\text{Al}_2\text{O}_3/\text{PbO}_2$  nanoparticles in shielding properties". *Journal of Materials Research and Technology*, 2020, 9(6), 13956–13962. <https://doi.org/10.1016/j.jmrt.2020.09.125>.
- [15]. S Ismail, S. F., Sahar, M. R., & Ghoshal, S. K., "Physical and absorption properties of titanium nanoparticles incorporated into zinc magnesium phosphate glass". *Materials Characterization*, 2016, 111, 177–182. <https://doi.org/10.1016/j.matchar.2015.11.030>.
- [16]. Juhim, F., Chee, F. P., Awang, A., Duinong, M., Rasmi, R., & Rumaling, M. I., "Review—Radiation Shielding Properties of Tellurite and Silicate Glass". *ECS Journal of Solid State Science and Technology*, 2022, 11(7), 76006. <https://doi.org/10.1149/2162-8777/ac81ea>.
- [17]. Kaky, K. M., Sayyed, M. I., Laariedh, F., Abdalsalam, A. H., Tekin, H. O., & Baki, S. O., "Structural, optical and radiation shielding properties of zinc boro-tellurite alumina glasses". *Applied Physics A: Materials Science and Processing*, 2018, 125(1), 0. <https://doi.org/10.1007/s00339-018-2329-3>.
- [18]. Zhou, Y., Baccaro, S., Cemmi, A., Yang, Y., & Chen, G., "Study on optical properties and  $\gamma$ -ray irradiation resistance of heavy metal oxide tellurite glasses". *Physica Status Solidi (C) Current Topics in Solid State Physics*, 2014, 12(1–2), 76–79. <https://doi.org/10.1002/pssc.201400148>.
- [19]. Sandhu, A. K., Singh, S., & Pandey, O. P., "Effect of neutron-irradiation on optical properties of  $\text{SiO}_2\text{-Na}_2\text{O-MgO-Al}_2\text{O}_3$  glasses". *Indian Journal of Physics*, 2009, 83(7), 985–991. <https://doi.org/10.1007/s12648-009-0058-3>.
- [20]. Cullity, B. D., & Stock, S. R. *Elements of X-Ray Diffraction*, Pearson Education Limited, 2014.
- [21]. Şakar, E., Özpolat, Ö. F., Alım, B., Sayyed, M. I., & Kurudirek, M., "Phy-X/PSD: Development of a user friendly online software for calculation of parameters relevant to radiation shielding and dosimetry". *Radiation Physics and Chemistry*, 2020, 166(July 2019). <https://doi.org/10.1016/j.radphyschem.2019.108496>.
- [22]. M Sarihan, M., "Simulation of gamma-ray shielding properties for materials of medical interest". *Open Chemistry*, 2022, 20(1), 81–87. <https://doi.org/10.1515/chem-2021-0118>.
- [23]. Rammah, Y. S., El-agawany, F. I., El, A. M. A., Yousef, E., & El-mesady, I. A., "Ionizing radiation attenuation competences of gallium germanate-tellurite glasses utilizing MCNP5 simulation code and Phy-X/PSD program". *Ceramics International*, 2020, 46(14), 22766–22773. <https://doi.org/10.1016/j.ceramint.2020.06.043>.
- [24]. Nidzam, N. N. S., Kamari, H. M., Sukari, M. S. M., Alauddin, F. A. M., Laoding, H., Azlan, M. N., Hann, S. W., Al-Hada, N. M., & Boukhris, I., "Comparison Study of Elastic, Physical and Structural Properties for Strontium Oxide and Manganese Oxide in Borotellurite Glasses for High Strength Glass Application". *Journal of Inorganic and Organometallic Polymers and Materials*, 2022, 32(1), 353–364. <https://doi.org/10.1007/s10904-021-02134-7>.
- [25]. Chee, F. P., Amir, H. F. A., & Salleh, S., "Simulation of ionizing radiation induced effects in nanoscale semiconductor material". *2011 IEEE Regional Symposium on Micro and Nanoelectronics, RSM 2011-Programme and Abstracts*, 2011, (September), 245–249. <https://doi.org/10.1109/RSM.2011.608833>.
- [26]. Sundaram, S. K., McCloy, J. S., Riley, B. J., Murphy, M. K., Qiao, H. A., Windisch, C. F., Shpotyuk, O., "Gamma radiation effects on physical, optical, and structural properties of binary as-S glasses". *Journal of the American Ceramic Society*, 2012, 95(3), 1048–1055. <https://doi.org/10.1111/j.1551-2916.2011.04938.x>.
- [27]. Ruller, J. A., & Friebele, E. J., "The effect of gamma-irradiation on the density of various types of silica". *Journal of Non-Crystalline Solids*, 1991, 136(1–2), 163–172. [https://doi.org/10.1016/0022-3093\(91\)90131-O](https://doi.org/10.1016/0022-3093(91)90131-O).
- [28]. Nabilah Razali, N. A., Mustafa, I. S., Azman, N. Z. N., Kamari, H. M., Rahman, A. A., Rosli, K., Taib, N. S., Tajuddin, N. A., "The Physical and Optical Studies of Erbium Doped Borosilicate Glass". *Journal of Physics: Conference Series*, 2018, 1083(1).

- <https://doi.org/10.1088/1742-6596/1083/1/012004>.
- [29]. Fares, H., Elhouichet, H., Gelloz, B., & Férid, M., "Surface plasmon resonance induced  $\text{Er}^{3+}$  photoluminescence enhancement in tellurite glass". *Journal of Applied Physics*, 2015, 117(19). <https://doi.org/10.1063/1.4921436>.
- [30]. Abou Hussein, E. M., Abdel Maksoud, M. I. A., Fahim, R. A., & Awed, A. S., "Unveiling the gamma irradiation effects on linear and nonlinear optical properties of  $\text{CeO}_2\text{-Na}_2\text{O-SrO-B}_2\text{O}_3$  glass". *Optical Materials*, 2021, 114(March), 111007. <https://doi.org/10.1016/j.optmat.2021.111007>.
- [31]. Nuclear Chemistry and Its Applications. Haïssinsky. M, Addison-Wesley, 1964.
- [32]. Halimah, M. K., Hasnimulyati, L., Zakaria, A., Halim, S. A., Ishak, M., Azuraida, A., & Al-Hada, N. M., "Influence of gamma radiation on the structural and optical properties of thulium-doped glass". *Materials Science and Engineering: B*, 2017, 226 (August), 158–163. <https://doi.org/10.1016/j.mseb.2017.09.010>.
- [33]. Rai, V. N., Raja Sekhar, B. N., Kher, S., & Deb, S. K., "Effect of gamma ray irradiation on optical properties of Nd doped phosphate glass". *Journal of Luminescence*, 2010, 130(4), 582–586. <https://doi.org/10.1016/j.jlumin.2009.10.034>.
- [34]. Sayyed, M. I., Issa, S. A. M., Büyükyıldız, M., & Dong, M., "Determination of nuclear radiation shielding properties of some tellurite glasses using MCNP5 code. *Radiation Physics and Chemistry*". *Radiation Physics and Chemistry*, 2018, 150 (April), 1–8. <https://doi.org/10.1016/j.radphyschem.2018.04.014>.
- [35]. Kebaili, I., Boukhris, I., Al-Buriahi, M. S., Alalawi, A., & Sayyed, M. I., "Ge-Se-Sb-Ag chalcogenide glasses for nuclear radiation shielding applications". *Ceramics International*, 2021, 47(1), 1303–1309. <https://doi.org/10.1016/j.ceramint.2020.08.251>.